

Evidence for a Zwitterionic transition state in double bond rotations within tungsten-vinyl complexes.

S. A. Gonsales,^a M. E. Pascualini,^a I. Ghiviriga,^a A. S. Veige

Table of Contents

1. General Considerations.....	S1
2. Synthesis of $[\text{CF}_3\text{-ONO}]\text{W}(\text{O})\{(\text{CH}_3)_3\text{CC}=\text{C}(\text{CH}_3)(\text{CH}_2\text{CH}_3)\}$ (4 and 4').....	S2
3. NMR Spectroscopic Data for complexes 4 and 4'.....	S4
4. Methyl exchange processes in 3_{syn} and 3_{anti}	S11
5. Methyl and ethyl exchange process in 4 and 4'.....	S14
6. DFT Calculations.....	S16
6.1. Mechanism 1: Through metallacycle formation.....	S16
6.2. Mechanism 2: Through double bond rotation.....	S17

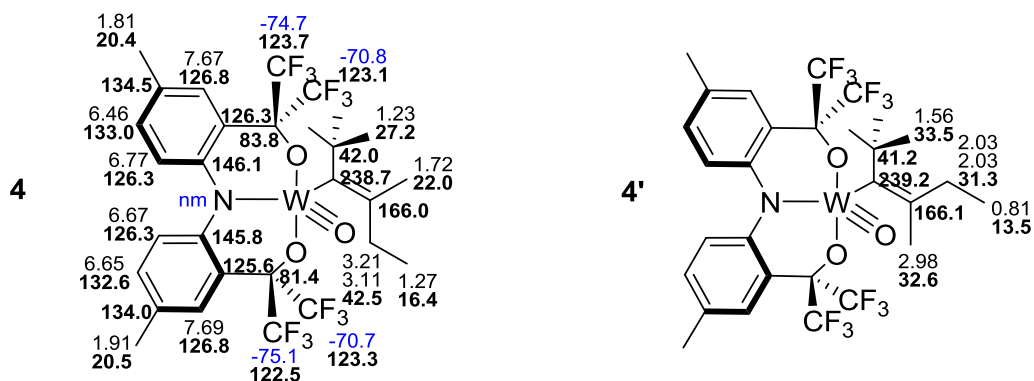
1. General Considerations.

Unless otherwise specified, all manipulations were performed under an inert atmosphere using glove-box techniques. Pentane, diethyl ether (Et_2O), tetrahydrofuran (THF) and benzene (C_6H_6) were dried using a GlassContour drying column. C_6D_6 (Cambridge Isotopes) was dried over sodium-benzophenone ketyl, distilled or vacuum transferred and stored over 4 Å molecular sieves. The ligand precursor $[\text{CF}_3\text{-ONO}]\text{H}_3$ (**1**), its corresponding tungsten-alkylidyne $[\text{CF}_3\text{-ONO}]\text{W}(\equiv\text{C}^t\text{Bu})(\text{THF})_2$ (**2**), and complex $[\text{CF}_3\text{-ONO}]\text{W}(\text{O})\{(\text{CH}_3)_3\text{CC}=\text{C}(\text{CH}_3)_2\}$ (**3**) were prepared according to published procedures.¹⁻⁴ ^1H and ^{13}C NMR spectra were obtained on Varian INOVA spectrometer, operating at 500 MHz for proton. The $^{19}\text{F}\{^1\text{H}\}$ spectra were obtained on a Varian Mercury spectrometer, operating at 300 MHz for proton. Chemical shifts, reported in δ (ppm), were referenced on the solvent, on the TMS scale for ^1H and ^{13}C and on the FCCL_3 for ^{19}F . Elemental analyses were performed at Complete Analysis Laboratory Inc., Parsippany, New Jersey.

2. Synthesis of $[\text{CF}_3\text{-ONO}]\text{W}(\text{O})\{(\text{CH}_3)_3\text{CC}=\text{C}(\text{CH}_3)(\text{CH}_2\text{CH}_3)\}$ (**4** and **4'**)

In a nitrogen filled glove box, 3.0 μL ($d=0.805$ g/mL, 0.035 mmol) of freshly distilled 2-butanone were added to a deuterated benzene solution of $[\text{CF}_3\text{-ONO}]\text{W}\equiv\text{CC}(\text{CH}_3)_3(\text{THF})_2$ (**2**) (0.030 g, 0.033 mmol), and a color change from light blue to dark green occurs instantaneously. The solvent was evaporated under reduced pressure. Yield (0.025g, 90%). Two isomers **4** and **4'** are instantaneously formed in a ratio of 3:1. ^1H NMR **4** ($\text{C}_6\text{D}_5\text{CD}_3$, 300 MHz, -60 $^\circ\text{C}$) δ (ppm): 7.69 (s, 1H, Ar-*H*), 7.67 (s, 1H, Ar-*H*), 6.77 (d, 1H, Ar-*H*), 6.67 (d, 1H, 2 Ar-*H*), 6.65 (d, 1H, Ar-*H*), 6.46 (d, 1H, Ar-*H*), 3.21 (m, 1H, $\text{WC}_\alpha=\text{C}_\beta(\text{CH}_3)(\text{CHH}'\text{CH}_3)$), 3.11 (m, 1H, $\text{WC}_\alpha=\text{C}_\beta(\text{CH}_3)(\text{CHH}'\text{CH}_3)$), 1.91 (s, 3H, Ar- CH_3), 1.81 (s, 3H, Ar- CH_3), 1.72 (s, 3H, $\text{WC}_\alpha=\text{C}_\beta(\text{CH}_3)(\text{CH}_2\text{CH}_3)$), 1.27 (t, 3H, $\text{WC}_\alpha=\text{C}_\beta(\text{CH}_3)(\text{CH}_2\text{CH}_3)$), 1.23 (s, 9H, ^tBu). $^{19}\text{F}\{^1\text{H}\}$ NMR **4** ($\text{C}_6\text{D}_5\text{CD}_3$, -60 $^\circ\text{C}$): $\delta = -70.7$ (q, 3F, $-\text{CF}_3$, $^4J = 9.2$ Hz), -70.7 (q, 3F, $-\text{CF}_3$, $^4J = 9.3$ Hz), -74.7 (q, 3F, $-\text{CF}_3$, $^4J = 9.1$ Hz), and -75.1 (q, 3F, $-\text{CF}_3$, $^4J = 9.2$ Hz). ^{13}C determined by ^1H - ^{13}C and ^{19}F - ^{13}C gHSQC and gHMBC experiments: **4** ($\text{C}_6\text{D}_5\text{CD}_3$, -60 $^\circ\text{C}$): $\delta = 238.7$ (s, WC_α), 166.0 (s, $\text{WC}_\alpha=\text{C}_\beta$), 146.1 (s, Ar C), 145.8 (s, Ar C), 134.5 (s, Ar C), 134.0 (s, Ar C), 133.0 (s, Ar C), 132.6 (s, Ar C), 126.8 (s, Ar C), 126.8 (s, Ar C), 126.3 (s, Ar C), 126.3 (s, Ar C), 126.3 (s, Ar C), 125.6 (s, Ar C), 123.7 (s, CF_3), 123.3 (s, CF_3), 123.1 (s, CF_3), 122.5 (s, CF_3), 83.8 (s, $\text{C}(\text{CF}_3)_2$), 81.4 (s, $\text{C}'(\text{CF}_3')_2$), 42.5 (s, $\text{WC}_\alpha=\text{C}_\beta(\text{CH}_3)(\text{CH}_2\text{CH}_3)$), 42.0 (s, $\text{C}_\alpha\text{C}(\text{CH}_3)_3$), 27.2 (s, $\text{WC}_\alpha\text{-C}(\text{CH}_3)_3$), 22.0 (s, $\text{WC}_\alpha=\text{C}_\beta(\text{CH}_3)(\text{CH}_2\text{CH}_3)$), 20.5 (s, Ar- CH_3), 20.4 (s, Ar'- CH_3'), 16.4 (s, $\text{WC}_\alpha=\text{C}_\beta(\text{CH}_3)(\text{CH}_2\text{CH}_3)$). ^1H NMR **4'** ($\text{C}_6\text{D}_5\text{CD}_3$, 300 MHz, -60 $^\circ\text{C}$) δ (ppm): 7.69 (s, 1H, Ar-*H*), 7.67 (s, 1H, Ar-*H*), 6.77 (d, 1H, Ar-*H*), 6.67 (d, 1H, 2 Ar-*H*), 6.65 (d, 1H, Ar-*H*), 6.46 (d, 1H, Ar-*H*), 2.98 (s, 3H, $\text{WC}_\alpha=\text{C}_\beta(\text{CH}_3)(\text{CH}_2\text{CH}_3)$), 2.03 (m, 1H,

$WC_\alpha=C_\beta(CH_3)(CHH'CH_3)$), 2.03 (m, 1H, $WC_\alpha=C_\beta(CH_3)(CHH'CH_3)$), 1.91 (s, 3H, Ar- CH_3), 1.81 (s, 3H, Ar- CH_3), 1.56 (s, 9H, t Bu), 0.81 (t, 3H, $WC_\alpha=C_\beta(CH_3)(CH_2CH_3)$). $^{19}F\{^1H\}$ NMR **4'** ($C_6D_5CD_3$, $-60^\circ C$): $\delta = -70.7$ (q, 3F, $-CF_3$, $^4J = 9.2$ Hz), -71.0 (q, 3F, $-CF_3$, $^4J = 9.3$ Hz), -74.7 (q, 3F, $-CF_3$, $^4J = 9.1$ Hz), and -75.1 (q, 3F, $-CF_3$, $^4J = 9.2$ Hz). ^{13}C determined by 1H - ^{13}C and ^{19}F - ^{13}C gHSQC and gHMBC experiments: **4'** ($C_6D_5CD_3$, $-60^\circ C$): $\delta = 239.2$ (s, WC_α), 166.1 (s, $WC_\alpha=C_\beta$), 146.1 (s, Ar C), 145.8 (s, Ar C), 134.5 (s, Ar C), 134.0 (s, Ar C), 133.0 (s, Ar C), 132.6 (s, Ar C), 126.8 (s, Ar C), 126.8 (s, Ar C), 126.3 (s, Ar C), 126.3 (s, Ar C), 126.3 (s, Ar C), 125.6 (s, Ar C), 123.7 (s, CF_3), 123.3 (s, CF_3), 123.1 (s, CF_3), 122.5 (s, CF_3), 83.8 (s, $C(CF_3)_2$), 81.4 (s, $C'(CF_3')_2$), 41.2 (s, $C_\alpha C(CH_3)_3$), 33.5 (s, $WC_\alpha-C(CH_3)_3$), 32.6 (s, $WC_\alpha=C_\beta(CH_3)(CH_2CH_3)$), 31.3 (s, $WC_\alpha=C_\beta(CH_3)(CH_2CH_3)$), 20.5 (s, Ar- CH_3), 20.4 (s, Ar'- CH_3'), 13.5 (s, $WC_\alpha=C_\beta(CH_3)(CH_2CH_3)$). Elemental analysis calcd. (%) for $C_{29}H_{29}F_{12}NO_3W$ (867.38 g/mol): C 40.91, H 3.43, N 1.65; Found: C 41.08, H 3.42, N 1.87.



3. NMR Spectroscopic Data for complexes **4** and **4'**

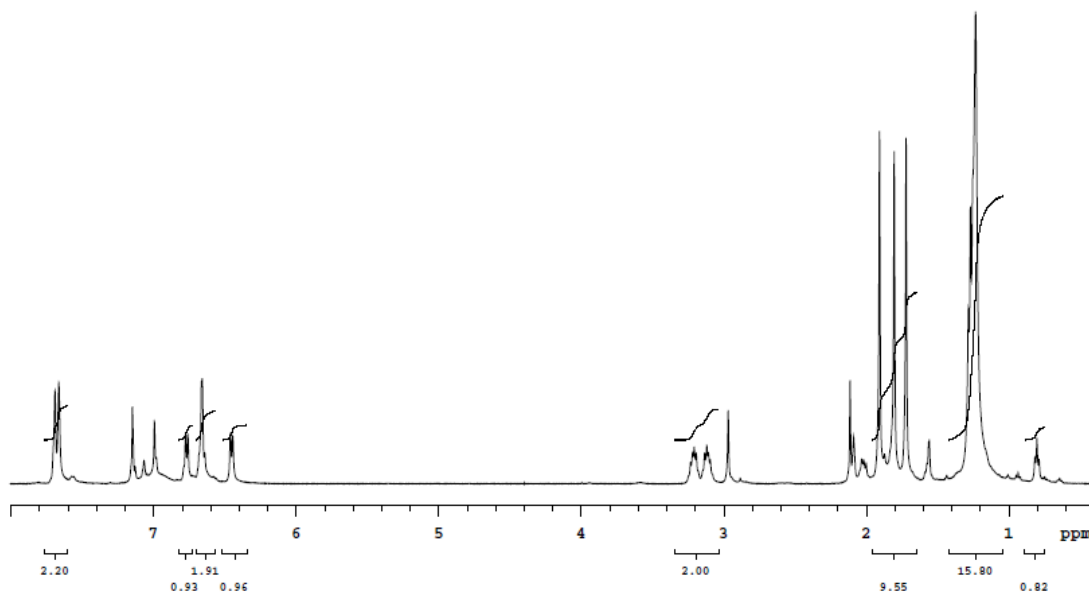


Figure S1. ¹H NMR spectrum of **4** and **4'** in C₆D₅CD₃ at -60 °C.

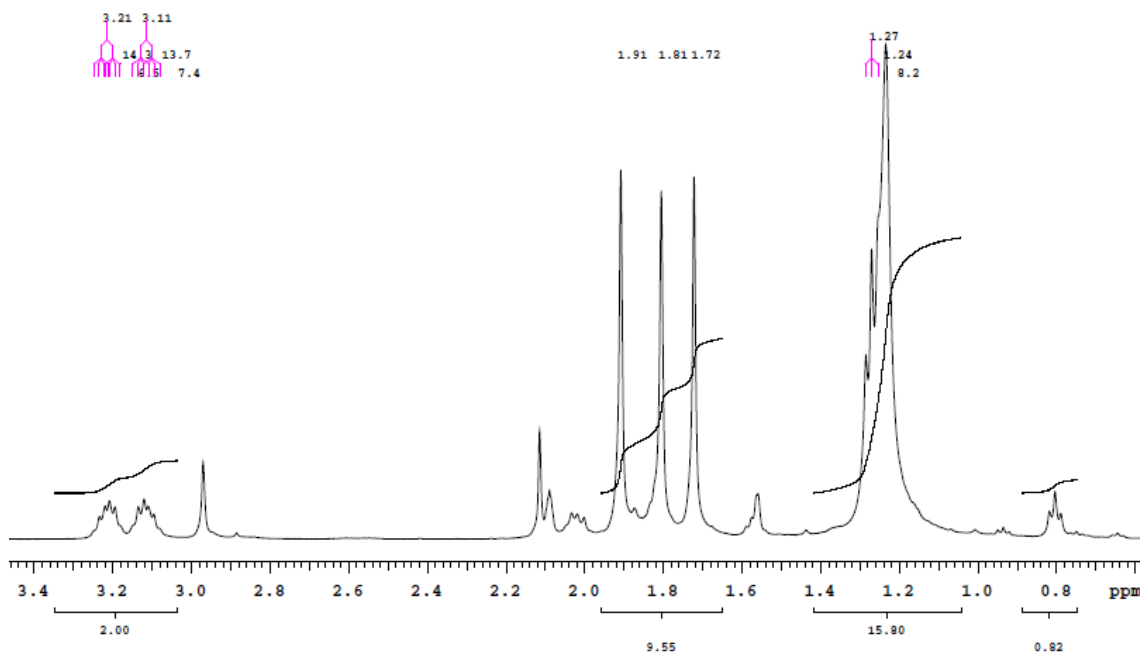


Figure S2. Expansion of ¹H NMR spectrum of **4** and **4'** in C₆D₅CD₃ at -60 °C.

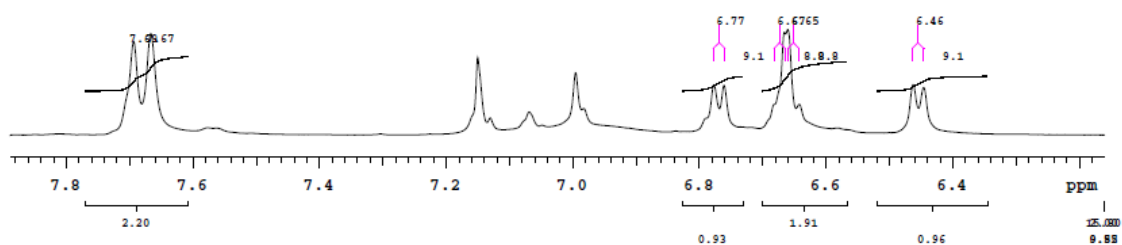


Figure S3. Expansion of ^1H NMR spectrum of **4** and **4'** in $\text{C}_6\text{D}_5\text{CD}_3$ at $-60\text{ }^\circ\text{C}$.

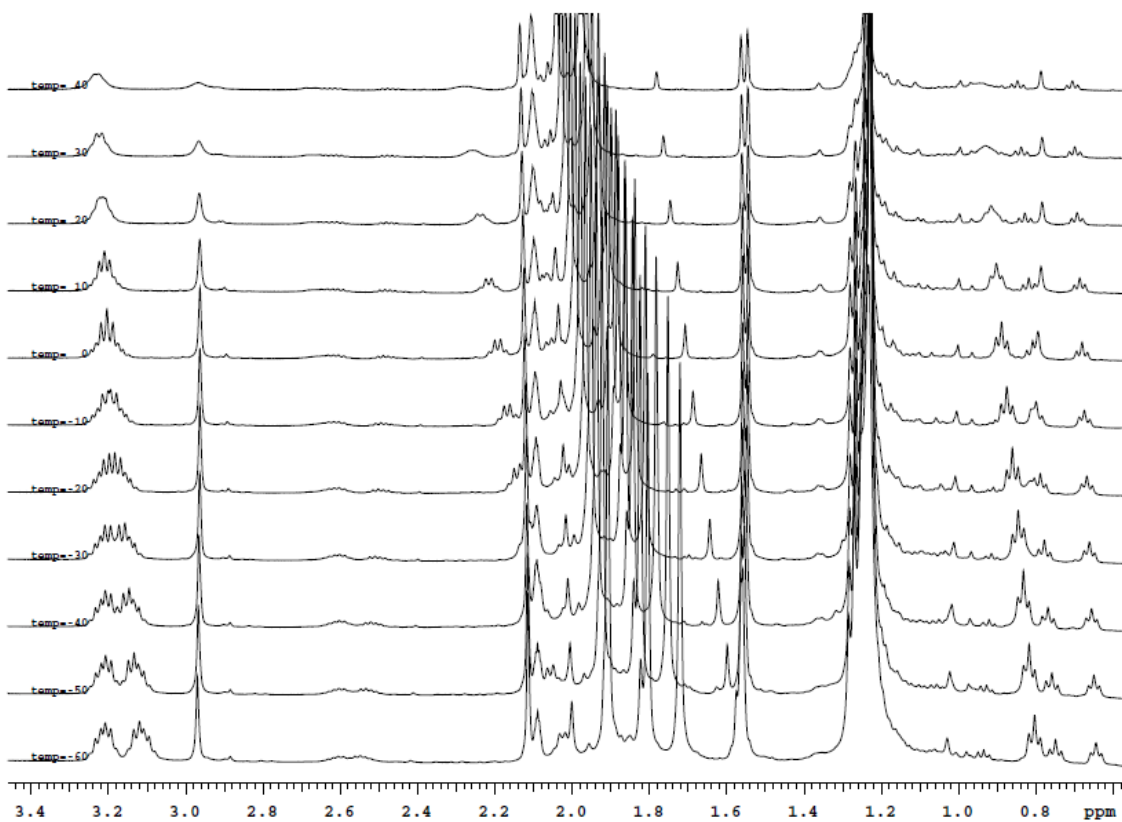


Figure S4. ^1H NMR spectrum of **4** and **4'** (aliphatic region) in $\text{C}_6\text{D}_5\text{CD}_3$, temperature array ($-60\text{ }^\circ\text{C}$ to $40\text{ }^\circ\text{C}$).

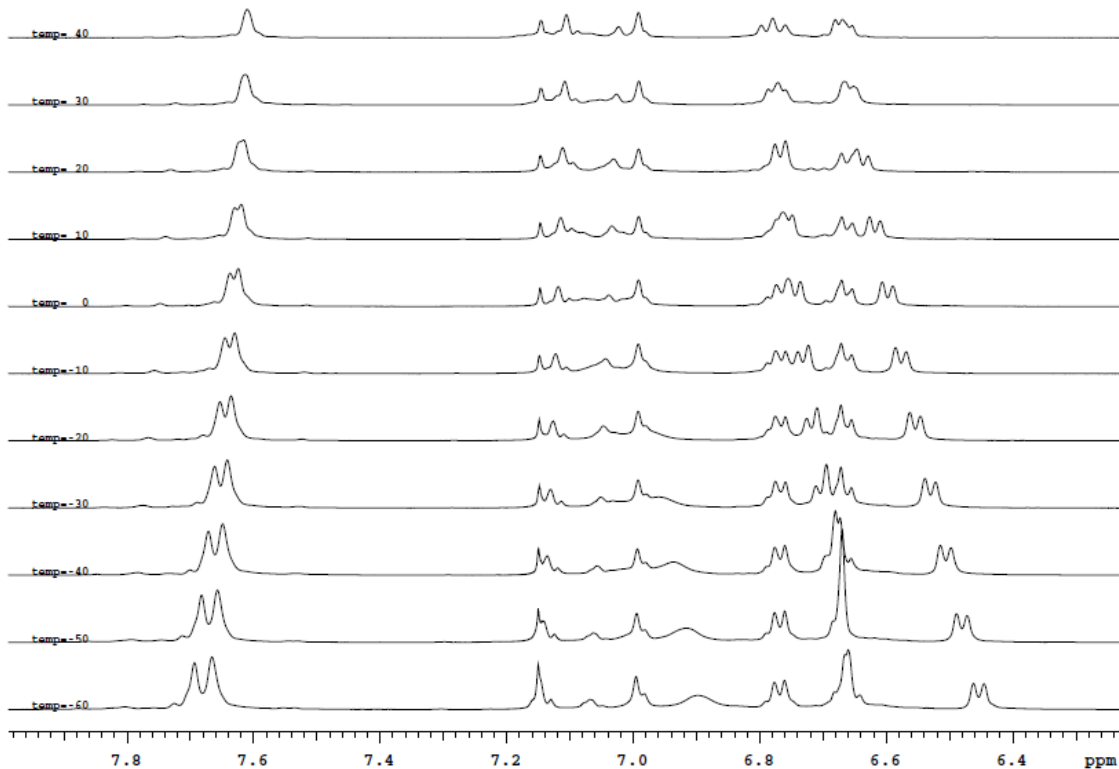


Figure S5. ^1H NMR spectrum of **4** and **4'** (aromatic region) in $\text{C}_6\text{D}_5\text{CD}_3$, temperature array (-60 °C to 40 °C).

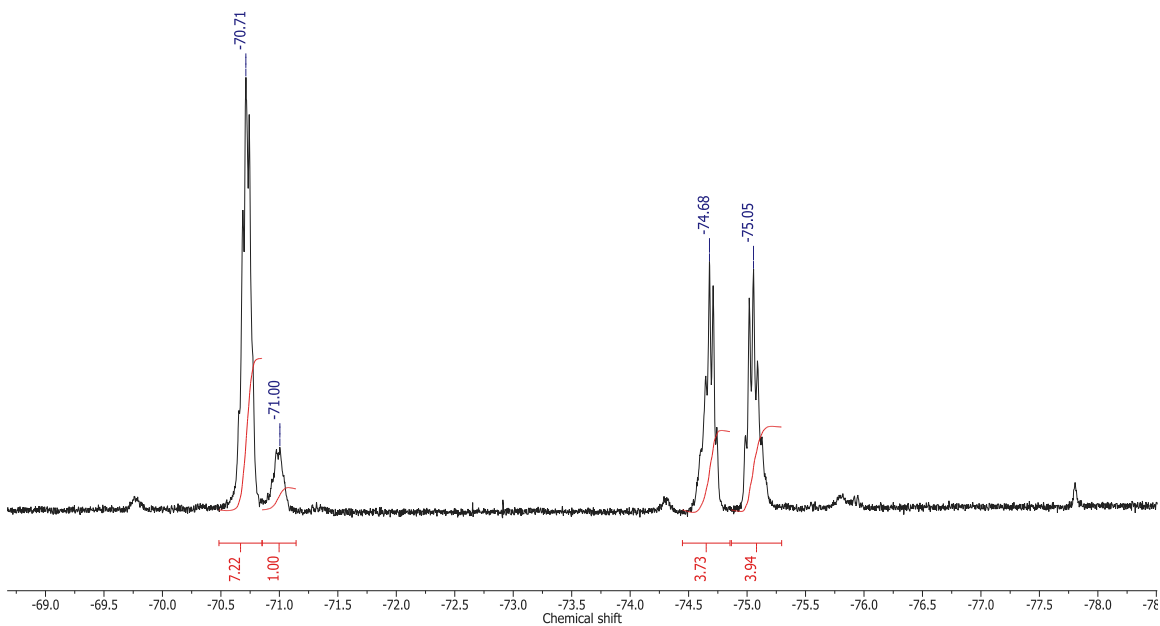


Figure S6. $^{19}\text{F}\{^1\text{H}\}$ NMR spectrum of **4** and **4'** in C_6D_6 .

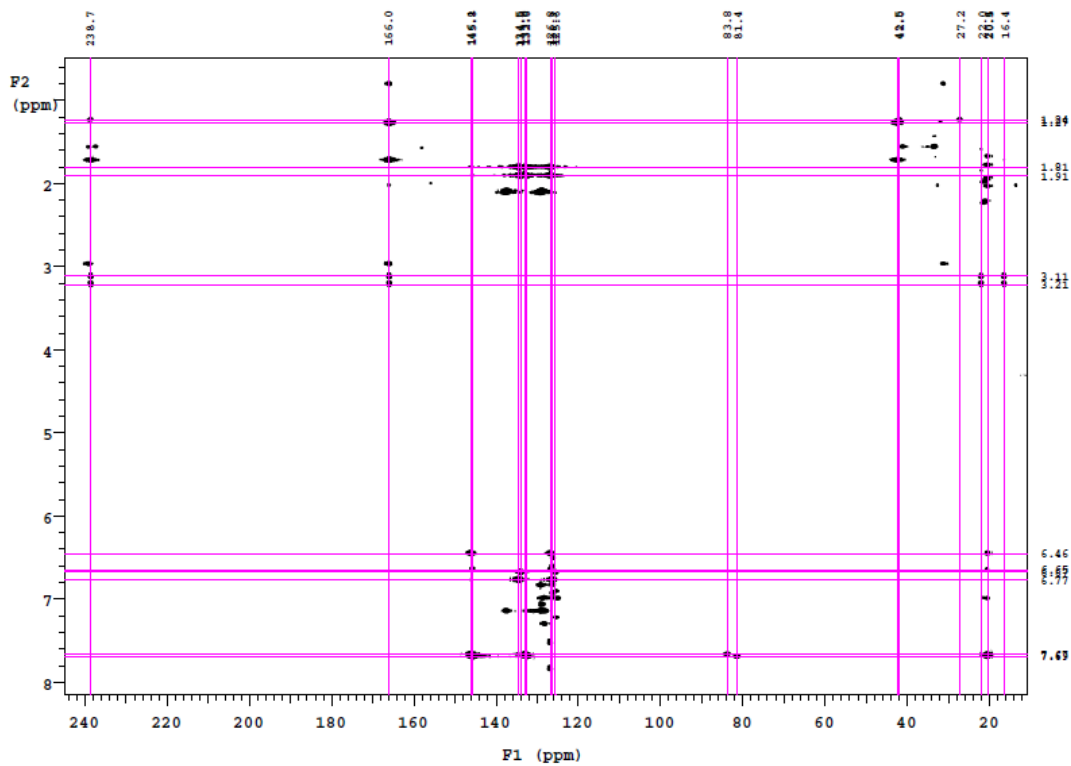


Figure S7. ^1H - ^{13}C gHMBC NMR spectrum of **4** and **4'** in $\text{C}_6\text{D}_5\text{CD}_3$ at $-60\text{ }^\circ\text{C}$.

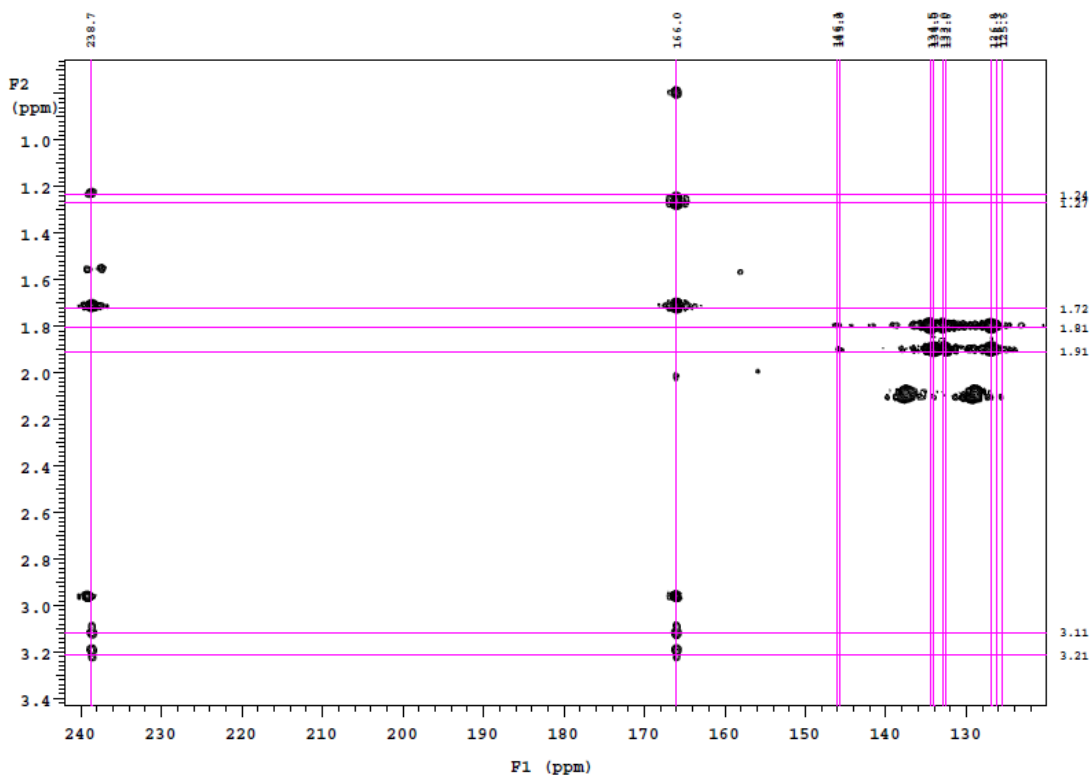


Figure S8. Expansion of ^1H - ^{13}C gHMBC NMR spectrum of **4** and **4'** in $\text{C}_6\text{D}_5\text{CD}_3$ at $-60\text{ }^\circ\text{C}$.

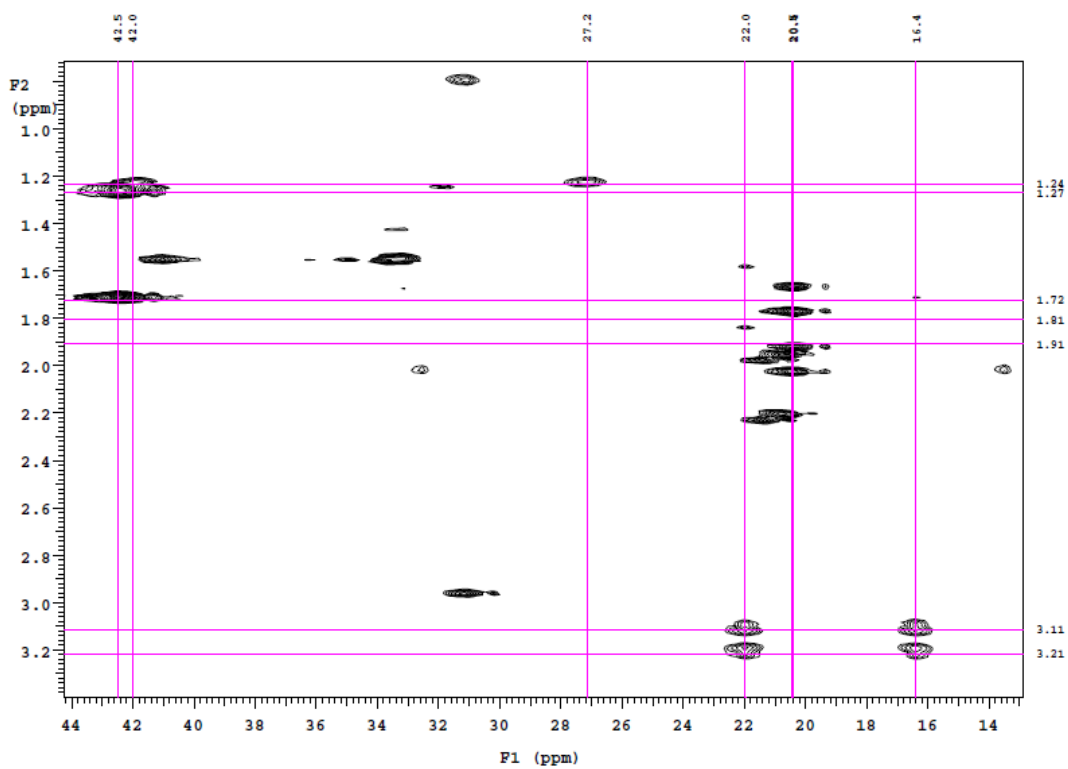


Figure S9. Expansion of ^1H - ^{13}C gHMBC NMR spectrum of **4** and **4'** in $\text{C}_6\text{D}_5\text{CD}_3$ at $-60\text{ }^\circ\text{C}$.

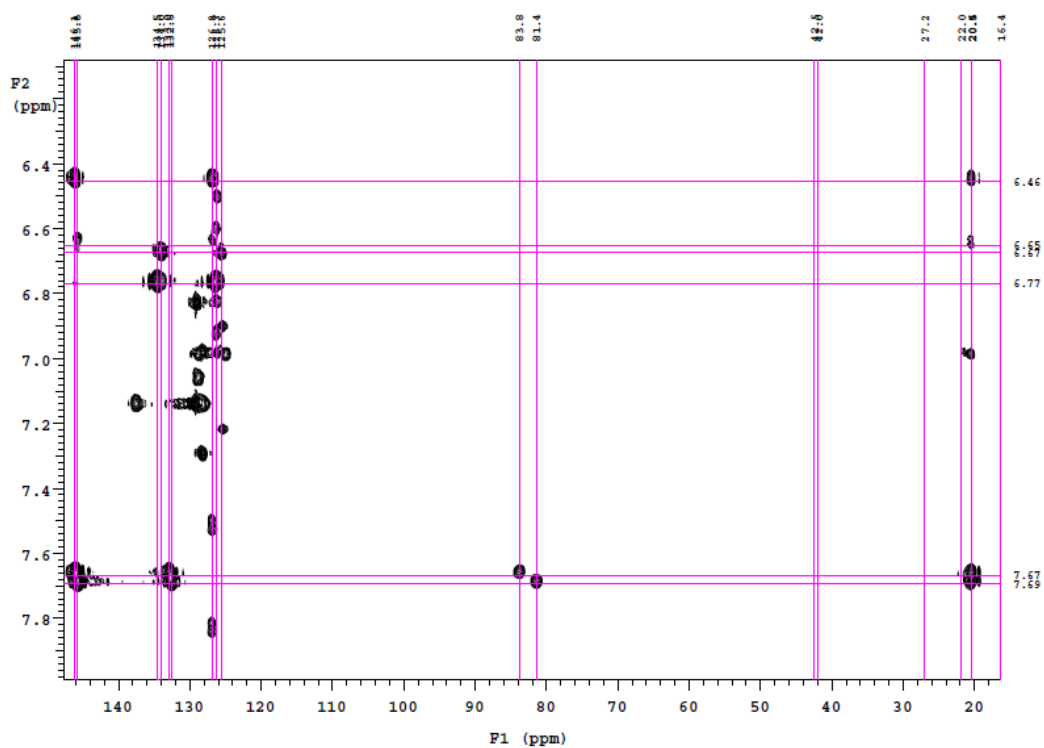


Figure S10. Expansion of ^1H - ^{13}C gHMBC NMR spectrum of **4** and **4'** in $\text{C}_6\text{D}_5\text{CD}_3$ at $-60\text{ }^\circ\text{C}$.

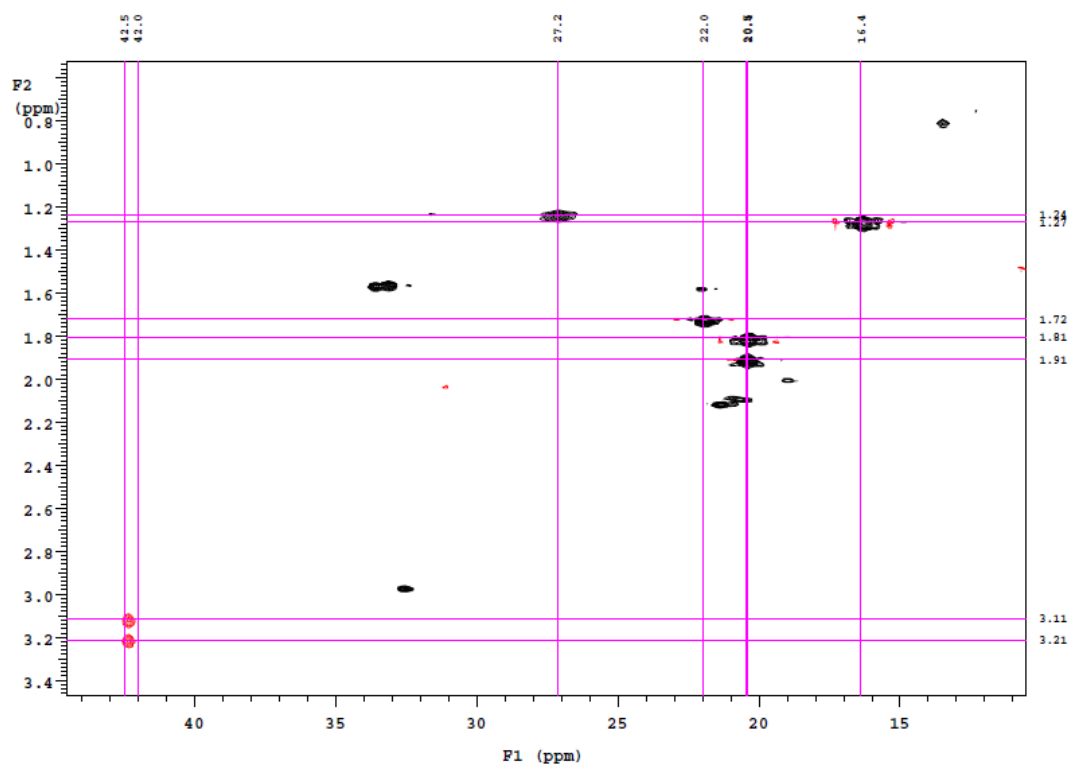


Figure S11. Expansion of ^1H - ^{13}C gHSQC NMR spectrum of **4** and **4'** in $\text{C}_6\text{D}_5\text{CD}_3$ at $-60\text{ }^\circ\text{C}$.

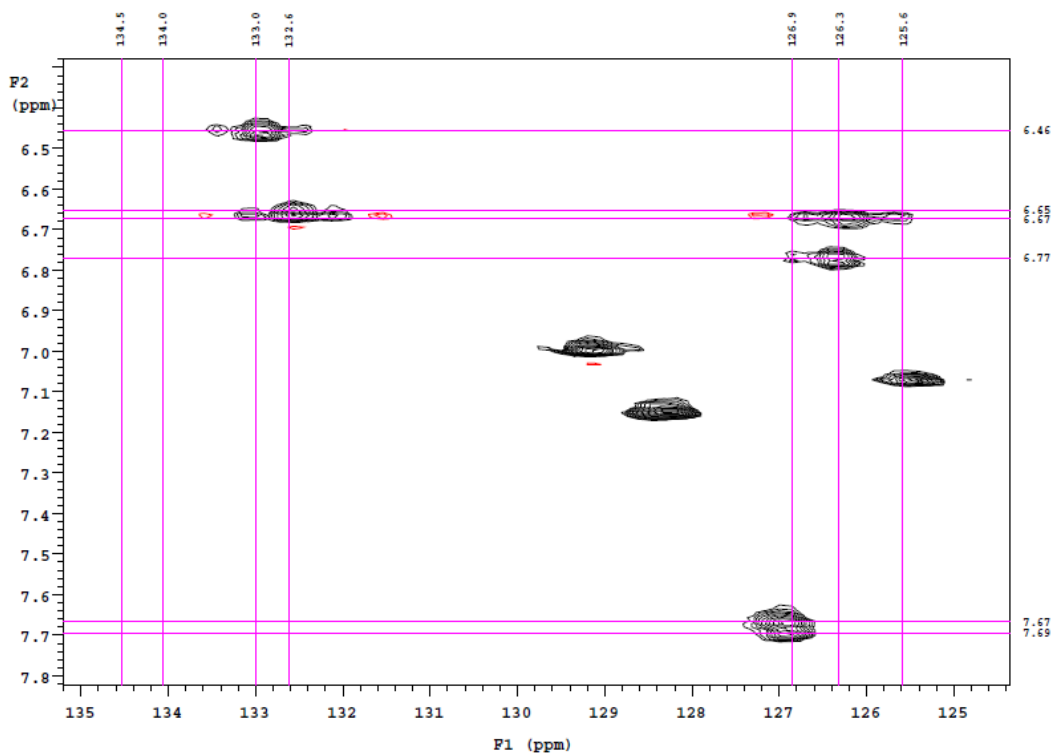


Figure S12. Expansion of ^1H - ^{13}C gHSQC NMR spectrum of **4** and **4'** in $\text{C}_6\text{D}_5\text{CD}_3$ at $-60\text{ }^\circ\text{C}$.

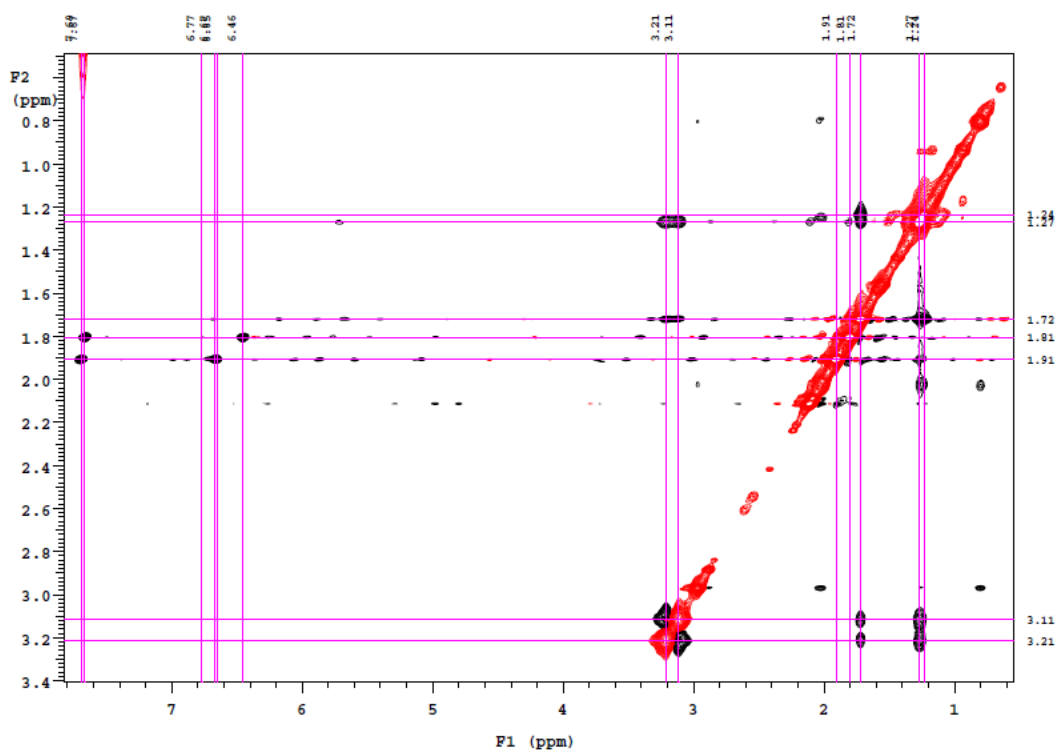


Figure S13. Expansion of ^1H - ^1H ROESY NMR spectrum of **4** and **4'** in $\text{C}_6\text{D}_5\text{CD}_3$ at $-60\text{ }^\circ\text{C}$.

4. Methyl exchange processes in 3_{syn} and 3_{anti}

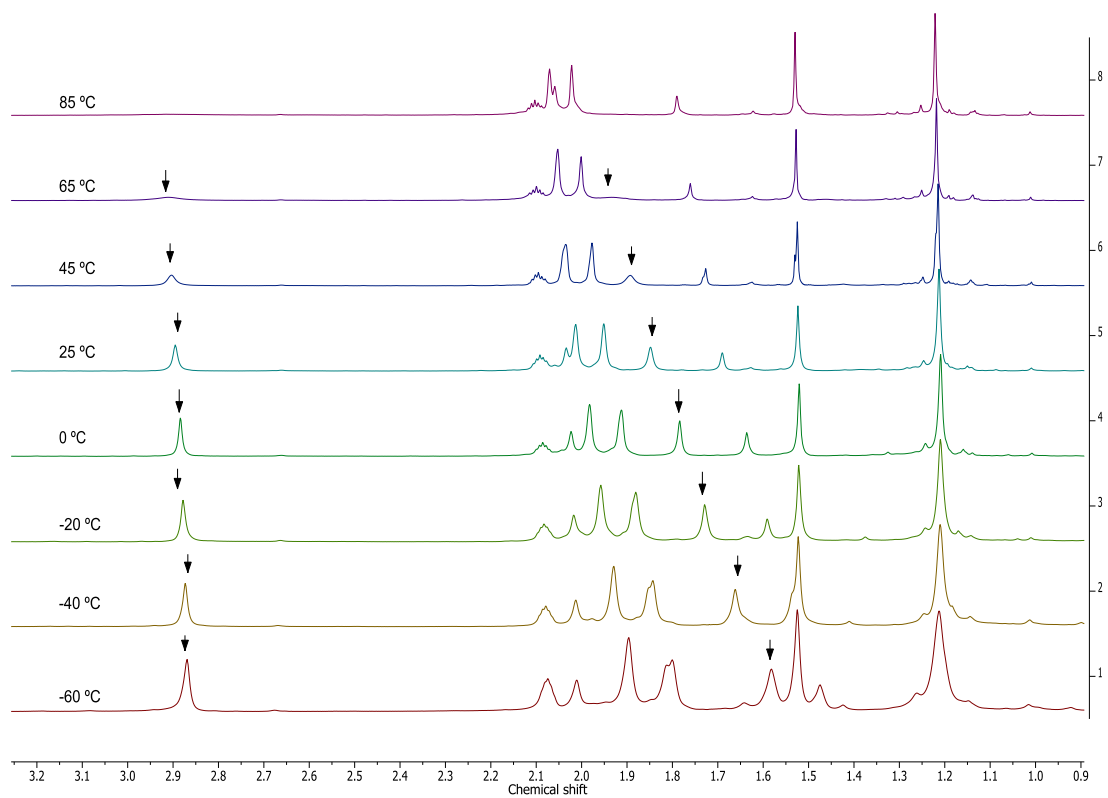


Figure S14. Aliphatic region VT ^1H NMR spectra of 3_{syn} in $\text{C}_6\text{D}_5\text{CD}_3$, methyl groups in exchange are highlighted.

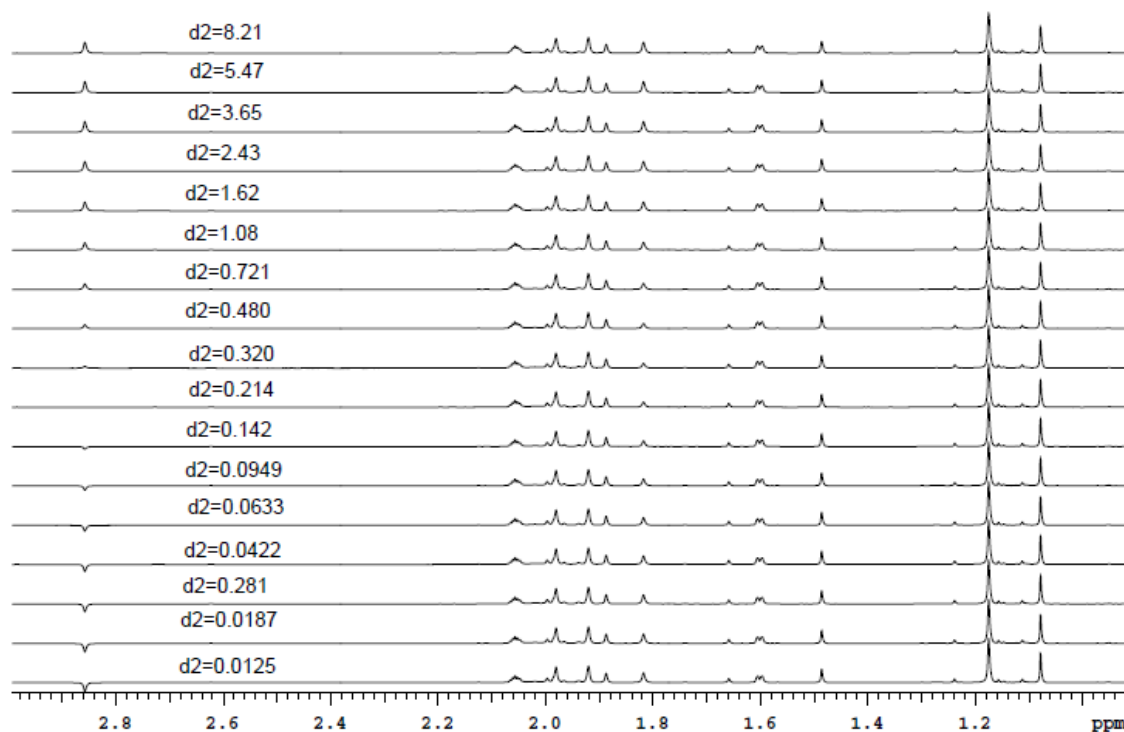


Figure S15. ^1H spectra of the selective-inversion-recovery experiment at 25 °C in $\text{C}_6\text{D}_5\text{CD}_3$. The spectra are taken d_2 seconds after the signal at 2.86 ppm is inverted. The intensity of the signal at 1.82 ppm evolves during d_2 as function of its T_1 and k_{exchange} .

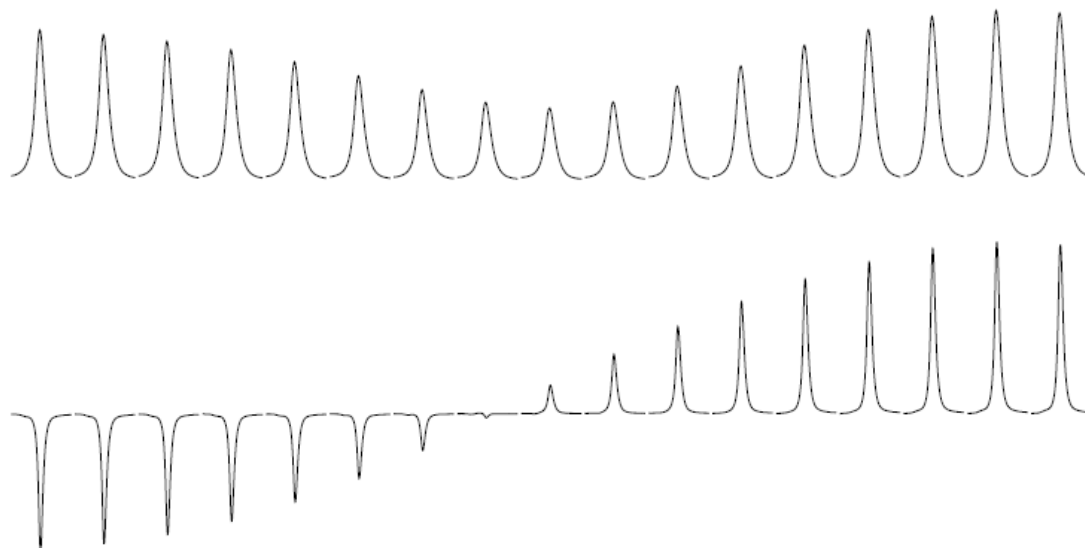


Figure S16. ^1H spectra of the selective inversion-recovery experiment, at 25 °C in toluene- d_8 . The spectra are taken d_2 seconds after the signal at 2.86 ppm (bottom row) is inverted. The intensity of the signal at 1.82 ppm (top row) evolves during d_2 as function of its T_1 and k_{exchange} .

The exchange rates for the reaction $\mathbf{3}_{\text{syn}}$ were determined at 12 equally spaced temperatures in the interval 0 – 55 °C, by iteratively fitting the exchange rate in the selective inversion-recovery experiments and the relaxation rates in the non-selective ones. The fit was done in Alex Bains' CIFIT program.⁵ Table S1 summarizes the different rates of exchange in different temperatures.

Table S1. Different rates of methyl exchange obtained at different temperatures

Temperature (K)	Rates k (s ⁻¹)
273.2	0.242
278.0	0.390
282.9	0.703
287.7	1.171
292.6	1.979
297.5	3.316
302.3	5.487
307.2	9.164
312.0	14.79
316.872	25.1481
321.7275	43.1729
326.583	67.8225

Using the Eyring equation, one can plot $\ln(k/T)$ versus $1/T$ to obtain thermodynamic parameters such as ΔH , ΔS and consequently ΔG for the methyl exchange process in $\mathbf{3}_{\text{syn}}$.

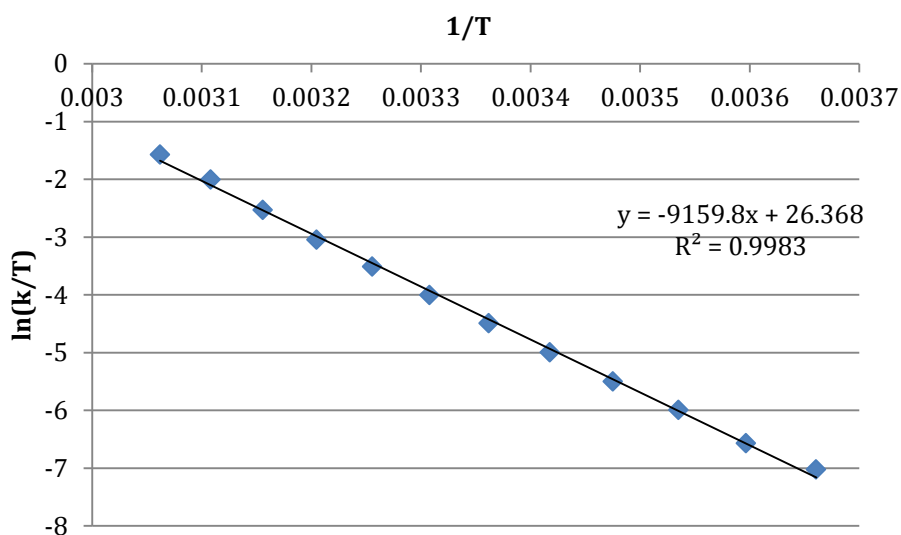


Figure S17. Plot of $\ln(k/T)$ versus $1/T$ for the methyl exchange process in complex $\mathbf{3}_{\text{syn}}$.

From the Eyring plot, we obtained a slope of $-9159.8 (\pm 121.2)$, and an intercept of $26.368 (\pm 0.406)$, which lead to $\Delta H = 18.2 \pm 0.2 \text{ kcal}\cdot\text{mol}^{-1}$, $\Delta S = 5.2 \pm 0.8 \text{ cal}\cdot\text{mol}^{-1}\cdot\text{K}^{-1}$, and $\Delta G = 16.6 \pm 0.3 \text{ kcal}\cdot\text{mol}^{-1}$ at $25 \text{ }^\circ\text{C}$ (298.15 K).

- **3_{anti}**

Exchange between the methyl groups was observed for **10_{anti}** at $95 \text{ }^\circ\text{C}$. Selective inversion of the resonance at 1.81 ppm leads to inversion of the resonance at 2.07 ppm (Figure S18).

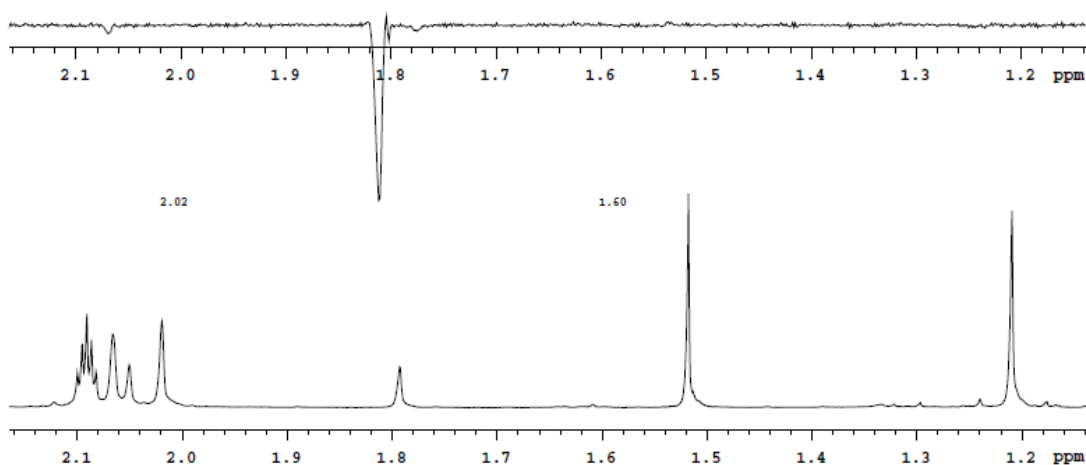


Figure S18. NOESY1D spectrum of a mixture of **3_{syn}** and **3_{anti}** at $95 \text{ }^\circ\text{C}$, in $\text{C}_6\text{D}_5\text{CD}_3$. Selective inversion of the methyl group from **3_{anti}** (1.81 ppm) leading to inversion of the other methyl group from **3_{anti}** at 2.07 ppm .

5. Methyl and ethyl exchange process in **4** and **4'**

Figure S19 and Figure S20 show the selective inversion-recovery experiments in which the resonance at $3.21\text{-}3.11 \text{ ppm}$ was selectively inverted, while the resonance at 2.03 evolves during d_2 as a function of its T_1 and k_{exchange} .

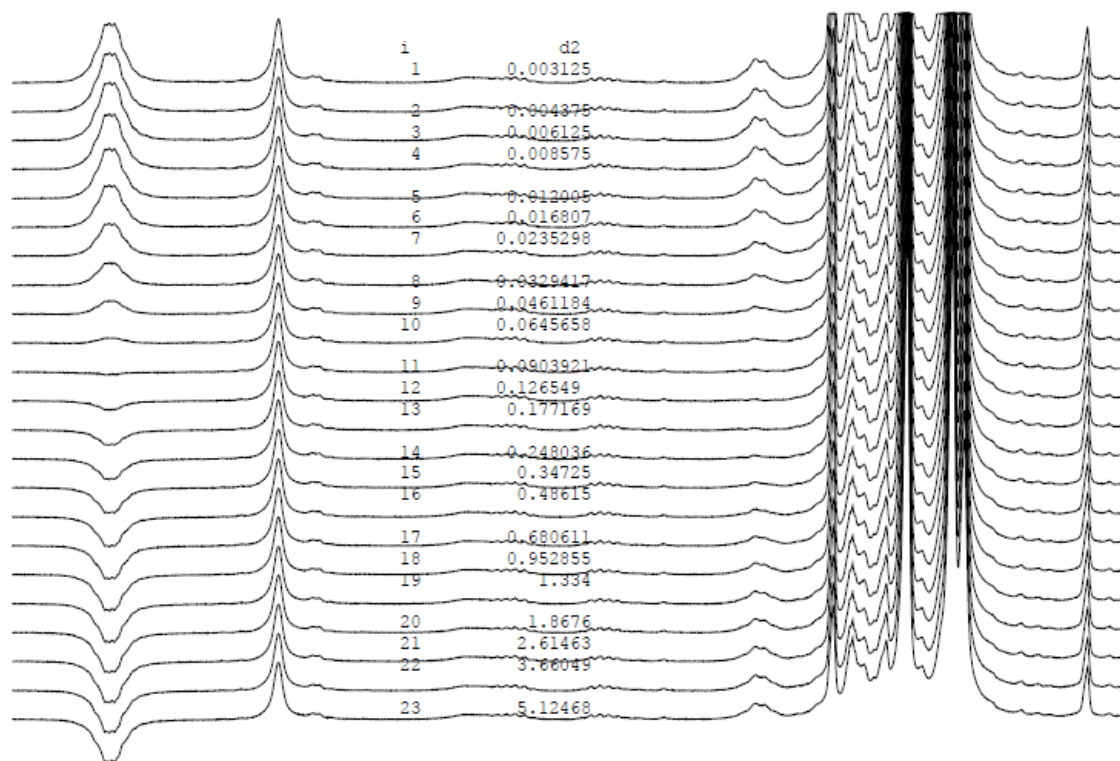


Figure S19. ^1H spectra of the selective inversion-recovery experiment of 4/4', at 20 °C in $\text{C}_6\text{D}_5\text{CD}_3$. The spectra are taken d2 seconds after the signal at 3.21-3.11 ppm is inverted. The intensity of the signal at 2.03 ppm evolves during d2 as a function of its T1 and k_{exchange} .

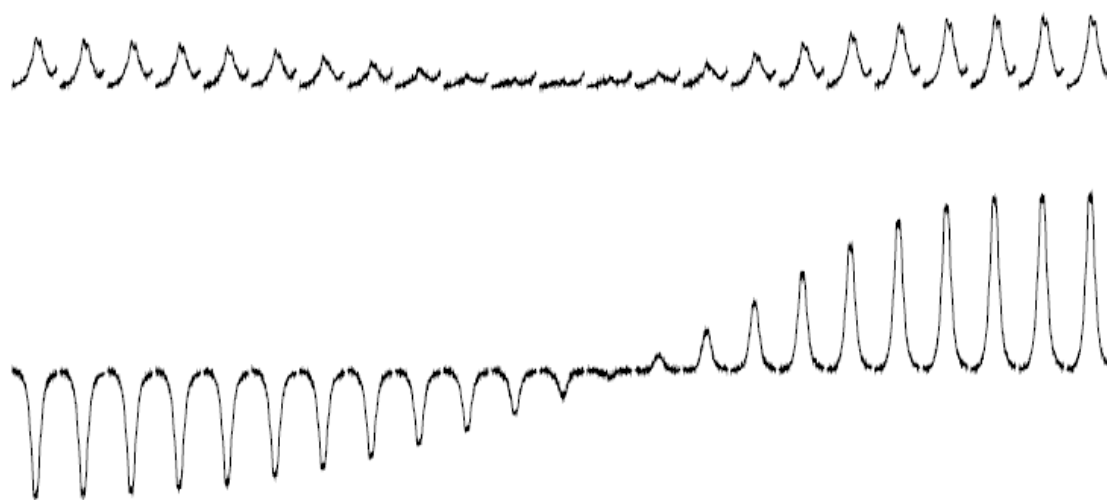


Figure S20. ^1H spectra of the selective inversion-recovery experiment of 4/4', at 20 °C in $\text{C}_6\text{D}_5\text{CD}_3$. The spectra are taken d2 seconds after the signal at 3.21-3.11 ppm (bottom) is inverted. The intensity of the signal at 2.03 ppm (top) evolves during d2 as a function of its T1 and k_{exchange} .

6. DFT Calculations

All density functional theory calculations were performed with the Gaussian 09 package⁶ at the B3LYP⁷⁻⁸ level of theory. The LANL2DZ basis set and an effective core potential were used for the W atom and 6-31G** for all other atoms. The geometries were optimized using atomic coordinates from the crystal structure as an initial guess when available. Solvent effects were incorporated using the polarizable continuum model with the corresponding dielectric constant. Geometry optimizations were followed by frequency calculations to confirm the absence of negative eigenvalues in the case of ground state (GS) configurations, or the presence of only one negative eigenvalue following the reaction coordinate in the case of transition states (TS).

6.1. Mechanism 1: Through metallacycle formation.

The initial geometry for the GS was derived from the crystal structure of $\mathbf{3}_{\text{syn}}$, while the initial guess for the intermediate (Int) was obtained by modifying the optimized GS. The initial geometry guess for the TS was obtained by performing a distance scan using the modredundant keyword starting from Int where the C-O bond was stretched from the value in optimized Int to the value in optimized GS. Frequency analysis confirmed the absence of negative eigenvalues for GS and Int, and the presence of a single negative eigenvalue in TS, which corresponds mainly to the stretching motion of the C-O bond. Figure S21 depicts the resulting energy surface.

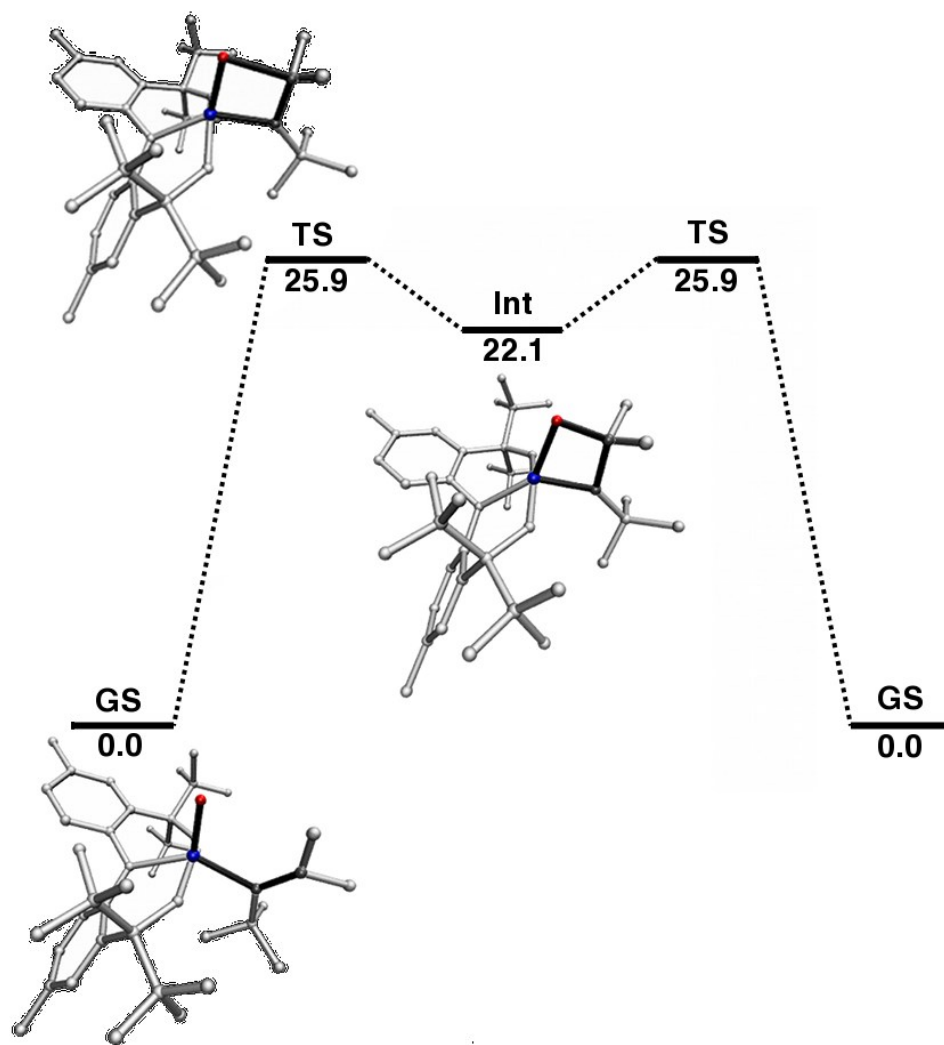


Figure S21. Calculated energy surface for the methyl exchange through the metallacycle formation mechanism at the B3LYP level of theory. Relative energies in kcal/mol.

6.2. Mechanism 2: Through double bond rotation

The initial geometry guess for the TS was obtained by performing a dihedral angle scan using the modredundant keyword starting from the GS (**3_{syn}**), where the WC=CC angle was rotated 180° in 10° increments. Starting from the final structure of this scan, the same procedure was conducted in the opposite direction. Figure S22 depicts the resulting energy profile, generated using symmetry considerations.

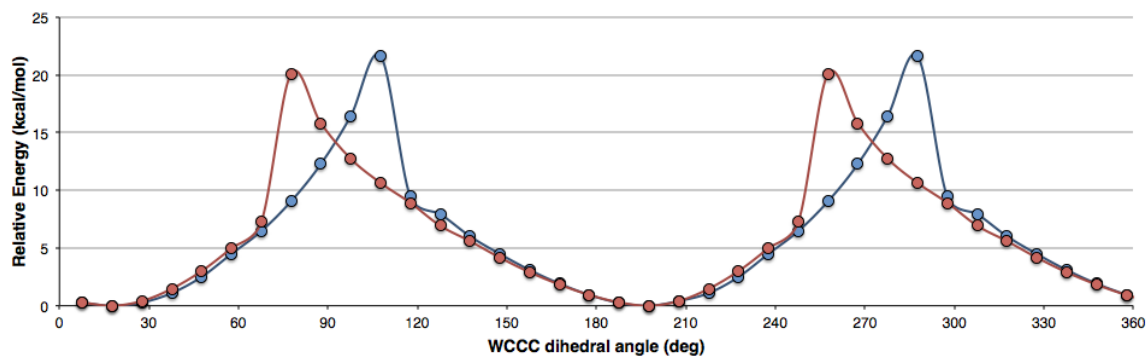


Figure S22. WC=CC dihedral angle scan starting from the optimized GS (blue) and in the reverse direction (red).

The structure closest to the intersection between the curves at 90° was used as the initial guess for a TS calculation. Frequency analysis confirmed the presence of a single negative eigenvalue in TS, which corresponds mainly to the rotation about the C=C bond. Figure S23 depicts the resulting energy surface.

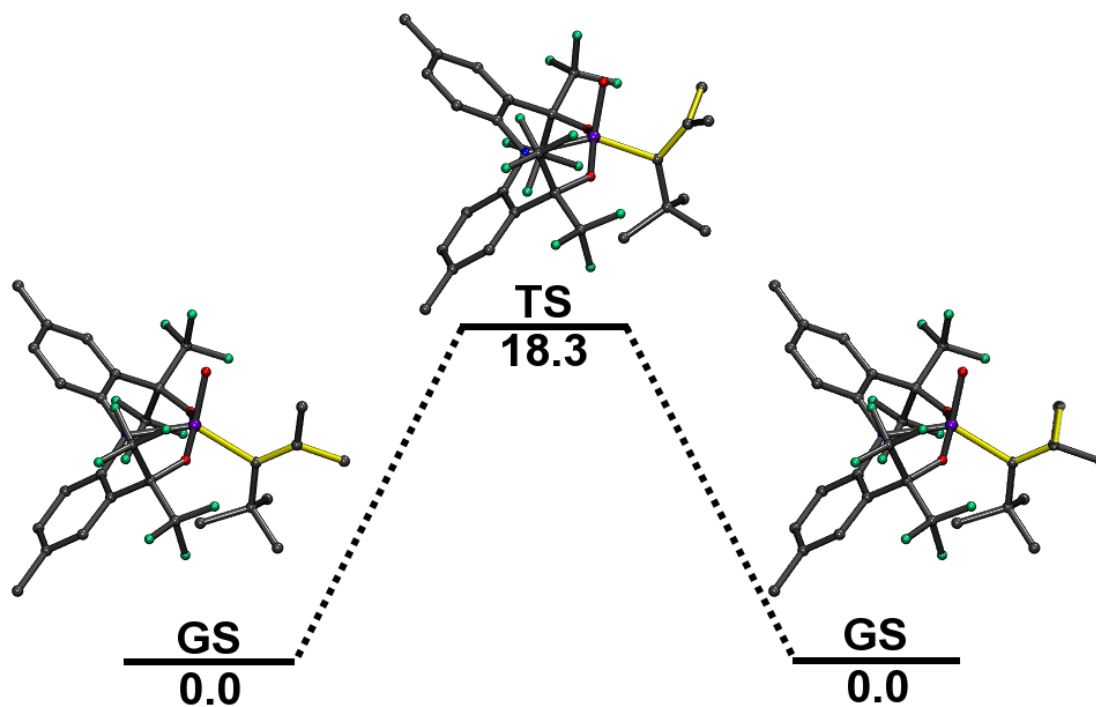


Figure S23. Calculated energy surface for the methyl exchange through double bond rotation at the B3LYP level of theory. The WC=CC angle is highlighted in yellow. Relative energies in kcal/mol.

The same procedure was applied to obtain the energy profile for WC=CC bond rotation in the 3_{anti} conformation. Figure S24 depicts the energy profile resulting from the dihedral angle scan, generated using symmetry considerations. Figure S25 depicts the energy surface obtained after optimizing the TS conformation.

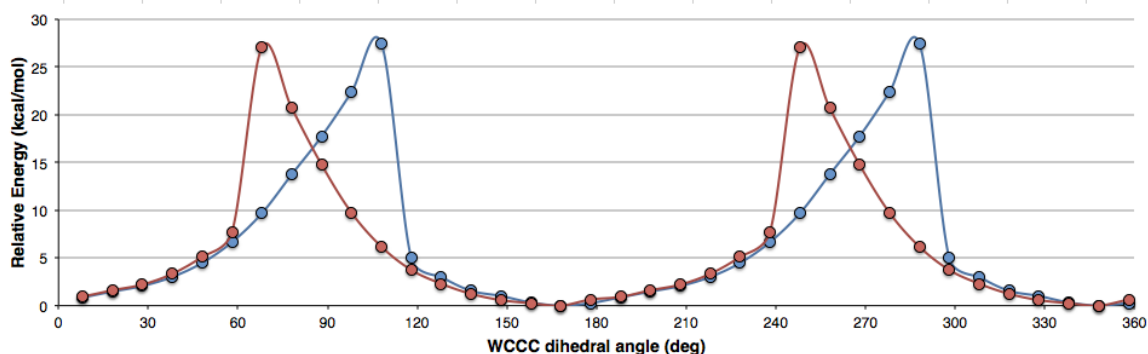


Figure S24. WC=CC dihedral angle scan starting from the 3_{anti} conformation (blue) and in the reverse direction (red).

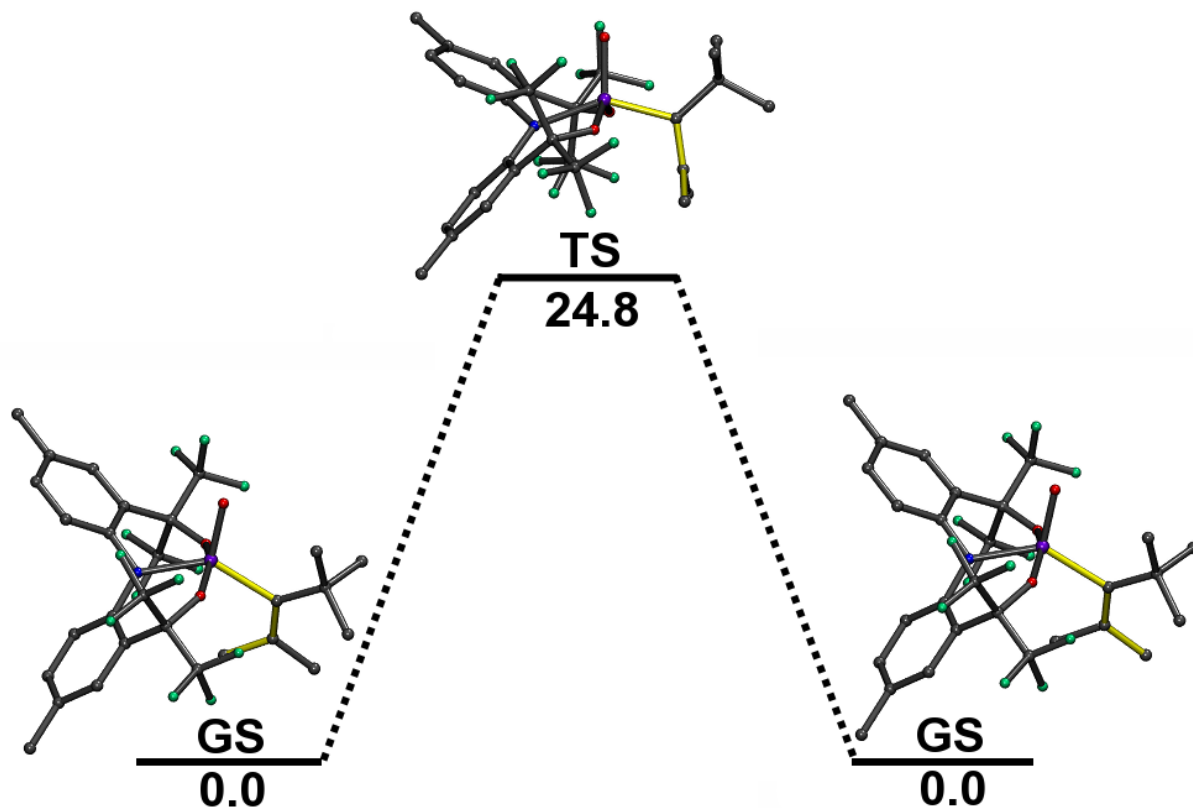


Figure S25. Calculated energy surface for the methyl exchange through double bond rotation in the 3_{anti} conformation at the B3LYP level of theory. The WC=CC angle is highlighted in yellow. Relative energies in kcal/mol.

- 1 M. E. O'Reilly, I. Ghiviriga, K. A. Abboud and A. S. Veige, *J. Am. Chem. Soc.*, 2012, **134**, 11185-11195.
- 2 M. E. O'Reilly, I. Ghiviriga, K. A. Abboud and A. S. Veige, *Dalton Trans.*, 2013, **42**, 3326-3336.
- 3 S. A. Gonsales, M. E. Pascualini, I. Ghiviriga, K. A. Khalil and S. A. Veige, *J. Am. Chem. Soc.*, 2015, **ASAP**.
- 4 S. A. Gonsales, M. E. Pascualini, I. Ghiviriga, K. A. Abboud and A. S. Veige, *Journal of the American Chemical Society*, 2015, **137**, 4840-4845.
- 5 A. D. Bain and J. A. Cramer, *J. Magn. Reson., Ser A*, 1996, **118**, 21-27.
- 6 M. J. Frisch, G. W. Trucks, H. B. Schlegel, G. E. Scuseria, M. A. Robb, J. R. Cheeseman, G. Scalmani, V. Barone, B. Mennucci, G. A. Petersson, H. Nakatsuji, M. Caricato, X. Li, H. P. Hratchian, A. F. Izmaylov, J. Bloino, G. Zheng, J. L. Sonnenberg, M. Hada, M. Ehara, K. Toyota, R. Fukuda, J. Hasegawa, M. Ishida, T. Nakajima, Y. Honda, O. Kitao, H. Nakai, T. Vreven, J. Montgomery, J. A., J. E. Peralta, F. Ogliaro, M. Bearpark, J. J. Heyd, E. Brothers, K. N. Kudin, V. N. Staroverov, T. Keith, R. Kobayashi, J. Normand, K. Raghavachari, A. Rendell, J. C. Burant, S. S. Iyengar, J. Tomasi, M. Cossi, N. Rega, J. M. Millam, M. Klene, J. E. Knox, J. B. Cross, V. Bakken, C. Adamo, J. Jaramillo, R. Gomperts, R. E. Stratmann, O. Yazyev, A. J. Austin, R. Cammi, C. Pomelli, J. W. Ochterski, R. L. Martin, K. Morokuma, V. G. Zakrzewski, G. A. Voth, P. Salvador, J. J. Dannenberg, S. Dapprich, A. D. Daniels, O. Farkas, J. B. Foresman, J. V. Ortiz, J. Cioslowski and D. J. Fox, Wallingford CT, 2013, pp. Gaussian, Inc.
- 7 A. D. Becke, *J. Chem. Phys.*, 1993, **98**, 5648-5652.
- 8 C. Lee, W. Yang and R. G. Parr, *Phys. Rev. B*, 1988, **37**, 785-789.